JOURNAL OF GUIDANCE, CONTROL, AND DYNAMICS
Vol. 17, No. 5, September–October 1994

Performance and Control of Proof-Mass Actuators Accounting for Stroke Saturation

Douglas K. Lindner,* Gregory A. Zvonar,† and Dusan Borojevic‡
Virginia Polytechnic Institute and State University, Blacksburg, Virginia 24061

We investigate the relationship between the parameters of a proof-mass actuator and the performance of that actuator within a vibration suppression loop for a flexible structure. We parametrize the model of the actuator in terms of the length of the proof-mass, the mass of the proof-mass, and the saturation force of the electromagnetic subsystem. The performance of the actuator within a vibration suppression control loop is characterized in terms of the relationship between the parameters and the structure's natural frequency. These results can be used to size a proof-mass actuator to maximize the operating region of the actuator and to maximize the ratio of the mass of the proof-mass to the total mass of the actuator.

Nomenclature

d	= stroke length, meters
$F_{\max}$	= maximum force available from the electromagnetic subsystem, N
$f_{\mathrm{pm}}(t)$	= force applied to the proof-mass by the electromagnetic subsystem, N
$f_{\mathrm{st}}(t)$	= $-f_{\mathrm{pm}}(t)$, reaction force applied to the structure, N
$G_{\mathrm{ry}}(s)$	= transfer function from actuator command, $r_{\mathrm{pm}}(t)$, to position of the proof-mass, $y_{\mathrm{pm}}(t)$, structure constrained to be stationary
$H(s)$	= force-to-velocity transfer function of the structure
K_{pa}	= forward path gain of the actuator control loop
K_{ps}	= gain of the position feedback vibration suppression control loop
K_{va}	= gain of the velocity feedback loop of the actuator
K_{vs}	= gain of the velocity feedback vibration suppression control loop
m	= mass of the proof-mass, kg
$\mathcal{OR}$	= operating region, a subset of the state space, meters
$r_{\mathrm{pm}}(t)$	= reference input to the actuator control system, volts
$t_s(x_0)$	= 1% settling time of the structure's position for the initial condition x_0, s
$v(t)$	= input signal to the power electronics, volts
$x(t)$	= state of the actuator/structure system, $x(t) \in R^4$, meters
$y_{\mathrm{pm}}(t)$	= displacement of the proof-mass, meters
$y_r(t)$	= relative displacement of the proof-mass from the structure, meters
$y_{\mathrm{st}}(t)$	= displacement of the structure, meters
ω_b	= saturation break frequency, rad/s
$\omega_{\mathrm{st}}, b, c$	= parameters of the structure, rad/s, N/m
$\zeta_{\mathrm{ed}}(x_0)$	= equivalent damping of the initial condition x_0
$\zeta_{\mathrm{PM}}(x_0)$	= performance function evaluated for the initial condition x_0

Introduction

A PROOF-mass actuator is a motor that accelerates a mass in a linear direction rather than in rotational motion. When this actuator is attached to a flexible structure, it can be modeled as a mass connected to the structure with an equivalent spring and damper. In response to an external command, the motor will impart a force to the proof-mass which in turn imparts a reaction force to the structure. In this configuration proof-mass actuators have been proposed[1–12] as actuators for the suppression of vibrations in flexible structures.

Proof-mass actuators are attractive for vibration suppression, in particular for space structures, because there is some indication that their weight-to-force ratio is superior to other actuators. To exploit this potential weight reduction, the actuator must be sized for a particular structure. This sizing is complicated because the proof-mass may run against its stops. We call the contact of the proof-mass with its stops "stroke saturation." Stroke saturation imparts shocks to the structure, and it can result in damage to the actuator. In this paper we consider design of the proof-mass actuator control system to avoid stroke saturation. These results can also be viewed as a step in the development of a criteria for the sizing of a proof-mass actuator, taking into account the stroke length of the actuator.

The capacity of the actuator is determined by the mass of the proof-mass, the stroke length, and the maximum force available from the electromechanical subsystem.[8–10] Using a one-mode model, we describe the relationship between these parameters, the natural frequency of the structure, and the operating region of the actuator. The results here represent an alternative approach to determining the operating region through an optimal control formulation.[5]

The actuator model discussed in this paper focuses on the system level characterization of proof-mass actuators. Our purpose is to describe the operational envelope of proof-mass actuators with respect to those parameters that are common to all realizations of proof-mass actuators. This model does not include detailed descriptions of nonlinearities in the device itself because these nonlinearities are realization dependent. The results in this paper generally apply to proof-mass actuators that rely on a specific realization of a proof-mass actuator.[1,2,4,6]

System Model

Actuator Model

In this paper we are concerned with the performance of a proof-mass actuator within a vibration suppression control loop for a flexible structure. We define a proof-mass actuator as any device that accelerates a (proof-) mass in linear motion and so generates a reaction force on the structure. The actuator is composed of two primary components: the proof-mass and the base. The proof-mass has mass m (kilograms), and length $2d$ (meters) which defines the range of linear motion. We say that the actuator has a "stroke" of d (meters). The base contains the power electronics and other components in a configuration that can apply a force to the proof-mass through electromagnetic coupling. The maximum force that can be applied by the electromechanical subsystem to the proof-mass is $F_{\max}$. These parameters are common to any physical realization of a proof-mass actuator.

Consider a proof-mass actuator attached to a flexible structure. The structure is modeled by one flexible mode. The model of this

Received Aug. 8, 1991; revision recieved Dec. 9, 1993; accepted for publication Dec. 9, 1993.

*Associate Professor, Bradley Department of Electrical Engineering. Member AIAA.

†Graduate Student, Bradley Department of Electrical Engineering.

‡Associate Professor, Bradley Department of Electrical Engineering.

system is shown in Fig. 1. A block diagram of the actuator and structure along with the control system components is shown in Fig. 2. To discuss the actuator model, we constrain the structure to be stationary. The input to the actuator is the voltage $v(t)$. This electrical signal is proportional to the force $f_{pm}(t)$ on the proof-mass generated by the electromechanical subsystem. The resulting displacement and velocity of the proof-mass are denoted $y_{pm}(t)$ and $\dot{y}_{pm}(t)$, respectively, and they are identified in Fig. 2.

The actuator contains two local loops to stabilize the proof-mass. The inner loop, labeled "Actuator Control Loop: Velocity Feedback," feeds back the velocity signal with a gain of K_{va}. The outer loop is a negative unity feedback of the position of the proof-mass (when $y_{st}(t) \equiv 0$). This loop is labeled the "Actuator Control Loop: Position Feedback." The two gains, K_{va} and K_{pa}, determine the transfer function $Y_{pm}(s)/R_{pm}(s)$ when the structure is constrained to be stationary. The outer loop represents the equivalent stiffness and the inner loop represents the equivalent damping of the proof-mass. The physical implementations of the actuator control loops may be mechanical or electronic or a combination of the two. The primary purpose of these loops is to manage the proof-mass, although they also affect the design of vibration suppression loops.[8]

Model of the Total System

From the full system in Fig. 2 we see that a force applied to the proof-mass, $f_{pm}(t)$, results in a reaction force on the structure, $f_{st}(t)$. At the location of the actuator attachment, the displacement of the structure is $y_{st}(t)$. The relationship between the applied force and resulting velocity of the structure is given by

$$\begin{aligned} \ddot{\eta}_{st}(t) + 2\zeta\omega_{st}\dot{\eta}(t) + \omega_{st}^2\eta(t) &= bf_{st}(t) \\ \dot{y}_{st}(t) = c\dot{\eta}(t), \quad y_{st}(t) &= c\eta(t) \end{aligned} \tag{1}$$

The transfer function $H(s)$ in Fig. 2 is calculated from Eq. (1). In the numerical simulations that follow the parameter values of the structure in Eq. (1) are $\omega_{st} = 8.2$ rad/s, $b = c = 0.024$, and $\zeta = 0.003$ (0.3% damping).[4]

We consider two feedback loops to effect the vibration suppression control loops. The first loop, labeled "Vibration Suppression Loop: Position Feedback" in Fig. 2, feeds back the position of the structure with a gain of K_{ps} to the actuator reference input, $r_{pm}(t)$. The second loop, labeled "Vibration Suppression Loop: Velocity Feedback" in Fig. 2, feeds back the velocity of the structure to the actuator with a gain of K_{vs}. The primary purpose of the vibration suppression loops is to suppress vibrations in the structure. The gains in the vibration suppression loops are chosen after the gains of the actuator control loops are fixed.

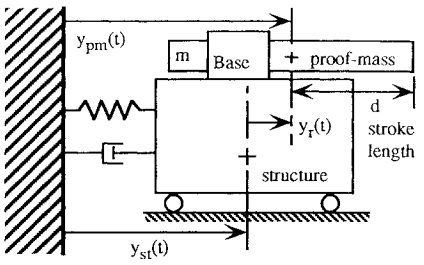

Fig. 1 Proof-mass actuator and a single degree-of-freedom model.

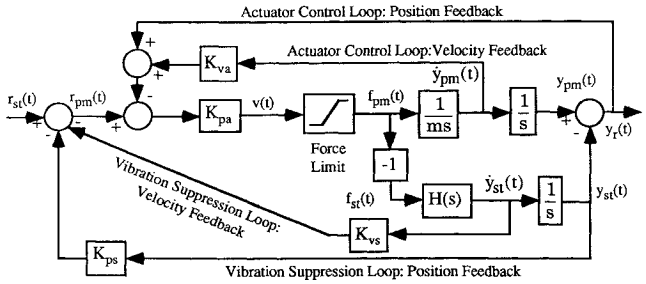

Fig. 2 Block diagram of a single mode structure with a proof-mass actuator.

Nonlinearities

In the analysis that follows, we consider two nonlinearities of the proof-mass actuator. The first nonlinearity models the maximum force available from the actuator electromagnetic subsystem, and it is described by a standard saturation nonlinearity:

$$f_{pm}(v) = \begin{cases} F_{max}, & v > F_{max} \\ v, & -F_{max} \le v \le F_{max} \\ -F_{max}, & v < -F_{max} \end{cases} \tag{2}$$

This nonlinearity is identified in Fig. 2 as the "Force Limit."

The second nonlinearity associated with the actuator is the stroke saturation; i.e., if the relative displacement of the proof-mass is greater than stroke d, $|y_r(t)| \ge d$, then the proof-mass will run against its stops. This nonlinearity is not shown explicitly in the block diagram of the system in Fig. 2. In this paper the stroke saturation provides a boundary in the state space of the system over which the proof-mass may not cross. We do not consider the dynamics of the structure after the proof-mass contacts its stops.

Parametrization of the Actuator

In this paper we investigate the performance of a proof-mass actuator operating within a vibration suppression control loop. In particular we will relate the parameters of the actuator (i.e., the mass of the proof-mass, the stroke length, and the maximum available force) to the ability of the actuator to meet the mission requirements of the structure. The nonlinearities of the actuator place an upper bound on the performance of the actuator. The actuator control loops determine the performance of the actuator within the vibration suppression control system. This analysis revolves around the relationship between the nonlinearities of the actuator, the frequency response of the actuator control loops, and the natural frequency of the mode of vibration of the structure. First we assume that the actuator control loops are open.

Stroke/Force Saturation Curve

Suppose that the motion of the proof-mass is

$$y_{pm}(t) = d \sin \omega t \tag{3}$$

Then the maximum instantaneous force imparted to the proof-mass is

$$F_{max\,stroke} = md\omega^2 \tag{4}$$

If the actuator is attached to a structure, Eq. (4) is approximately true, assuming the mass of the structure is much greater than the mass of the proof-mass.[8] The frequency-dependent curve (4) is plotted in Fig. 3 on a log-log scale, and it is labeled the "stroke saturation curve." In particular, the stroke saturation curve relates the stroke length d to the dynamic response of the proof-mass.

The second force constraint is the maximum force that can be supplied by the electromechanical subsystem, F_{max}. Assuming the signals are sinusoidal, the limitation on the signals of the actuator imposed by this nonlinearity is frequency independent. Hence, this constraint is a horizontal line shown in Fig. 3 as the force saturation curve.

The saturation break frequency ω_b is the frequency at which the maximum force output from the motion of the proof-mass in Eq. (4) is equal to F_{max},

$$\omega_b = \sqrt{F_{max}/md} \tag{5}$$

The saturation break frequency is identified in Fig. 3. At frequencies below the saturation break frequency the maximum force output is determined by the product of the stroke length and the mass, md. The scalar md is called the "mass/stroke constant." Above the saturation break frequency the maximum force output is determined by the maximum available force from the electromechanical subsystem, F_{max}. These two force constraints can be combined together to form the stroke/force saturation curve, also shown in Fig. 3.

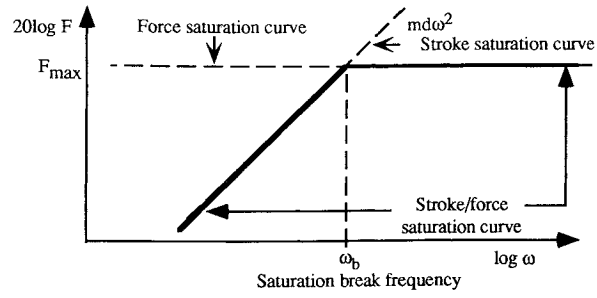

Fig. 3 Stroke/force saturation curve and actuator frequency response.

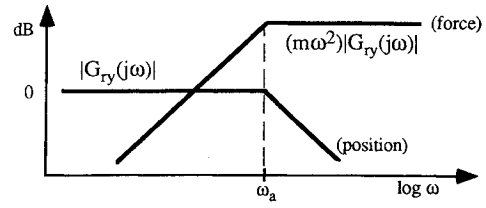

Fig. 4 Bode plots of $Y_{pm}(s)/R_{pm}(s)$ and $F_{pm}(s)/R_{pm}(s)$.

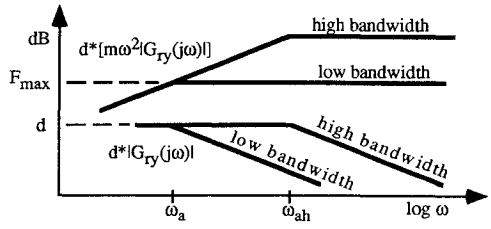

Fig. 5 Amplitudes of the position and force time responses.

Actuator Bandwidth

The stroke/force saturation curve can be related to the parameters and control loops of the actuator by appealing to the concepts of steady-state frequency response. During this discussion we assume that the actuator's control loops are closed. The transfer function from command input $r_{pm}(t)$ to position of the proof-mass $y_{pm}(t)$ is

$$\frac{Y_{pm}(s)}{R_{pm}(s)} = \frac{(K_{pa}/m)}{s^2 + K_{va}(K_{pa}/m)s + (K_{pa}/m)} = G_{ry}(s) \qquad (6)$$

In the design of the actuator control loops, we are to select the two parameters K_{pa} and K_{va} in Eq. (6). For reasons that will be made clear below, we choose the poles of the transfer function to make this transfer function maximally flat. Then the design of the actuator control loops reduces to the selection of the bandwidth of Eq. (6) through the selection of K_{pa}.

The straight-line approximation of the magnitude Bode plot for the transfer function in Eq. (6) is shown in Fig. 4. The actuator break frequency ω_a for the transfer function in Eq. (6) is

$$\omega_a = \sqrt{(K_{pa}/m)} \qquad (7)$$

The transfer function from the command input signal, $r_{pm}(t)$, to the force exerted on the proof-mass, $f_{pm}(t)$, is

$$\frac{F_{pm}(s)}{R_{pm}(s)} = (ms^2)G_{ry}(s) \qquad (8)$$

The magnitude Bode plot of Eq. (8) is also shown in Fig. 4. Note that these two Bode plots are related by the dynamics of the proof-mass, a relationship that is unaltered by the control loops.

The input signal to the actuator is given by

$$r_{pm}(t) = d \sin \omega t \qquad (9)$$

The steady-state displacement of the proof-mass is

$$y_{pm}(t) = d(|G_{ry}(j\omega)|) \sin(\omega t + \theta_{ry}) \qquad (10)$$

The straight-line approximation to the amplitude of the time response in Eq. (10) as a function of frequency is plotted in Fig. 5 on a log-log scale. For the command signal in Eq. (9) the force exerted on the proof-mass is given by

$$f_{pm}(t) = (d)|(m\omega^2)G_{ry}(j\omega)| \sin(\omega t + \theta_{ry}) \qquad (11)$$

The amplitude of this force applied to the proof-mass is also shown in Fig. 5.

The shape of the curves in Fig. 5 is determined by the transfer functions in Eqs. (6) and (8). The break frequency of these curves is determined by the break frequency of the actuator ω_a in Eq. (7). In Fig. 5 we have shown the amplitude of the time responses in Eqs. (10) and (11) for two different actuator break frequencies. In the first case we have chosen the actuator break frequency to be equal to the saturation break frequency,

$$\sqrt{(K_{pa}/m)} = \omega_a = \omega_b = \sqrt{(F_{max}/md)} \qquad (12)$$

These curves are labeled "low bandwidth." We have also shown these curves when the actuator break frequency is greater than the saturation break frequency, $\omega_{ah} > \omega_b$. These curves are labeled "high bandwidth."

First we consider the low-bandwidth curves. In the frequency band below the actuator break frequency, $\omega < \omega_a$, the control loops of $G_{ry}(s)$ in Eq. (6) are configured so that the Bode plots in Fig. 4 are flat at 0 dB. Here the position of the proof-mass tracks the command input signal. For the input signal in Eq. (9) the full stroke of the proof-mass is used. The amplitude of the displacement of the proof-mass is shown in Fig. 5. If the command signal's amplitude is allowed to exceed the stroke length d the actuator will saturate in stroke.

For frequencies above the break frequency, $\omega_a < \omega$, the proof-mass will generate a constant amplitude force on the structure as shown by the Bode plot in Fig. 4. For the input signal in Eq. (9), the amplitude of the resulting force signal is shown in Fig. 5, labeled "low bandwidth." The amplitude of the force depends on the actuator control loops as shown by Eqs. (8) and (11). This amplitude is exactly the maximum force capacity of the actuator. This relationship can be traced back to the selection of the actuator break frequency (choice of K_{pa}) to match the saturation break frequency of the actuator, ω_b, in Eq. (12).

We could attempt to improve the performance of the actuator by increasing the actuator break frequency, say,

$$\omega_{ah} = k\sqrt{(F_{max}/md)}, \quad k > 1 \qquad (13)$$

The resulting curves in Figs. 4 and 5 are labeled "high bandwidth." At frequencies below ω_b in Eq. (13), the actuator response is unchanged. At frequencies above this break frequency, however, the forces that are commanded are above the actuator capacity and the actuator will saturate in force. In the worst case the proof-mass will saturate in stroke.[8]

Summary

We have considered two different designs of the actuator control loops. First, we selected K_{pa} so that the break frequency of the actuator is matched to the saturation break frequency of the actuator. For the full stroke command in Eq. (9) the amplitude of the force

$$d \cdot |(m\omega^2)G_{ry}(j\omega)| \qquad (14)$$

will match the stroke/force saturation curve in Fig. 3 over the entire frequency band. Second, we considered the selection of K_{pa} such that the actuator break frequency was greater than the saturation break frequency. While the resulting amplitude of the position matched the stroke saturation curve, the actuator was driven into force saturation above the saturation break frequency. Hence, the saturation break frequency imposes a bound on the bandwidth of the actuator control loops. It also follows from this analysis that if the bandwidth of the actuator is selected to fall below the satura-

tion break frequency, then the force capacity of the actuator will be underutilized.

The correspondence between Eq. (14) and the stroke/force saturation curve establishes a relationship between the parameters of the actuator and its control loops, and the nonlinearities of the actuator. Next, we will compare the closed-loop performance of several actuators with different saturation break frequencies. Note that the actuator saturation break frequency in Eq. (7) only changes when the ratio of the maximum force to the mass/stroke constant changes. Scaling both quantities by the same factor leaves the saturation break frequency constant.

Performance Criteria

Mission Requirements of the Structure

We consider the selection of a proof-mass actuator for the vibration suppression control system in a flexible structure. We assume that the mission requirements for the structure are given as a minimum allowable damping (5%) in the structural modes of interest over the largest possible operating region. The actuator is to be selected so that it has the authority to meet the damping specifications, but it does not add excessive mass to the structure.

Damping

We consider nonlinear models of a proof-mass actuator attached to a flexible structure. If a set of initial conditions is close to the origin the system is completely linear so the usual definition of damping applies. As the norm of the initial condition increases the structure will enter into nonlinear behavior due to the force saturation of the actuator. In the nonlinear region we define the damping as follows. We let $t_s(x_0)$ be the 1% settling time of the structure's position $y_{st}(t)$ corresponding to the initial condition x_0. Define the equivalent damping $\zeta_{ed}(x_0)$ as

$$\zeta_{ed}(x_0) = \frac{-\ln 0.01}{\omega_{st} t_s(x_0)} \tag{15}$$

For a linear system this definition of damping will coincide with the usual definition of damping for all initial conditions.

Operating Region

The actuator's operating region is determined by the nonlinearities of the actuator. For a given set of initial conditions, we examine the time response of the relative position of the structure and the proof-mass. If the relative position is less than the stroke length of the actuator for $t \geq 0$, the actuator will not saturate in stroke and we say that the initial condition is in the operating region of the actuator. The states of our model are

$$x = [y_{pm} \quad \dot{y}_{pm} \quad y_{st} \quad \dot{y}_{st}]^T \tag{16}$$

The operating region $\mathcal{OR}$ is the set of initial conditions where

$$\mathcal{OR} = \left\{ x_0 = x(0) \mid \max_{t \geq 0} |y_r(t)| < d \right\} \tag{17}$$

We assume that the mission requirements preclude stroke saturation of the actuator because shocks are imparted to the structure and damage may occur to the actuator itself. By insisting that the actuator not saturate in stroke, we have defined hard boundaries for the operating system.

On an absolute scale we assume that the actuator can meet the damping specification in the mission requirements of the structure for some choice of actuator parameters. (The actuator placement, not considered in this paper, also affects the ability of the actuator to achieve specified damping levels.) For all actuators with a standard saturation characteristic, Eq. (2), there is an inverse relationship between the vibration loop gain and the size of the operating region. As the loop gain increases, size of the operating region decreases. In our discussion we normalize the vibration suppression loop gains so that near the origin the damping imparted to the structural mode is 5% for all closed loop systems. A suitable gain for the vibration loop, K_{ps} or K_{vs} in Fig. 2, can always be found, because near the origin the system is completely linear.[8] The size of the operating region will depend on the actuator's parameters and the actuator control loops. We will use the size of the actuator's operating region as a basis of comparison of actuator performance.

Performance Function

The equivalent damping captures the effect of the force saturation nonlinearity. The stroke saturation is captured by the operating region. To combine the two measures of equivalent damping and the operating region we define the performance function ζ_{PM}:

$$\zeta_{PM}: R^4 \to R; \zeta_{PM}(x_0) = \begin{cases} \zeta_{ed}(x_0), & x_0 \in \mathcal{OR} \\ 0, & x_0 \notin \mathcal{OR} \end{cases} \tag{18}$$

Given two actuators with approximately the same equivalent damping profile, the actuator with the largest operating region is considered more desirable.

Mass Efficiency

This research was motivated by a desire to develop a sizing criteria for proof-mass actuators. Here we consider sizing an actuator with the minimum total mass, but with enough authority to meet the damping specifications. We assume that the structure's parameters in Eq. (1) are fixed. After the actuator is attached to the structure, we assume that 5% damping can be imparted to the structure using the vibration suppression control loops. This assumption implies that the actuator has a certain level of authority. One way to parametrize this authority is to assume that the maximum force available from the electromechanical subsystem of the actuator is fixed. Here we will use $F_{max} = 30$ N. This parametrization essentially determines a lower bound on the total mass of the actuator.

The distribution of the mass of each of the components of the actuator must be considered so that each component of the actuator is being used to full capacity most of the time. For a given total mass the authority of the actuator is divided between the electromagnetic force applied to the proof-mass and the mass and stroke length of the proof-mass. At high frequencies, the authority of the actuator is determined by maximum force available from the electromechanical subsystem, F_{max}. An increase in the maximum electromagnetic force applied to the proof-mass will increase the authority of the actuator. This increase in the authority will also increase the mass of the base, because the base of the actuator contains the electromechanical subsystem. At low frequencies, the authority of the actuator is determined by the mass of the proof-mass and the stroke length. As mass of the proof-mass and its stroke length is increased, evidently the authority of the actuator is increased.

We define the mass efficiency of the actuator as the ratio of the mass of the proof-mass to the mass of the entire actuator. The mass efficiency measures the relative mass contributions of the electromagnetic force and the proof-mass.

Summary

Given the three actuators parameters m, d, and F_{max}, the stroke/force saturation curve is completely determined. Then the actuator loop gains are chosen such that the frequency response of the transfer function in Eq. (6) matches the stroke/force saturation curve. Finally, the vibration suppression loops are chosen such that the structure's mode has 5% damping in the linear region around the origin.

Given the controlled structure, the actuator's performance can be evaluated through simulation using the performance function in Eq. (18). The larger the operating region the better the performance of the actuator. In this way the actuator can be sized by the three parameters m, d, and F_{max}. These parameters are to be chosen such that the operating region is as large as possible so that the actuator is being used to its full capacity most of the time over the largest possible operating region, the total mass is minimized, and the mass efficiency is as close to unity as possible.

Actuator Parameter Selection for the Vibration Loops

Actuator Performance Functions

In this section we investigate the performance of a proof-mass actuator within a vibration suppression loop for a flexible structure. Because ω_b is determined by the parameters of the actuator we

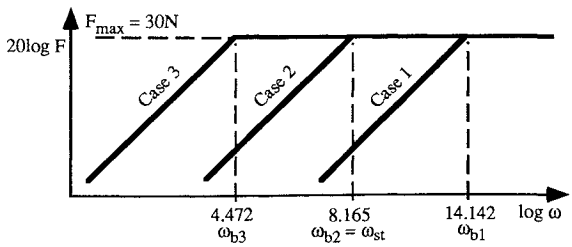

Fig. 6 Stroke/force saturation curves.

can investigate the performance of actuators of different sizes for a given structure by studying the performance of the actuators as ω_b varies with respect to ω_{st}. We consider three values of ω_b shown in Table 1. The gains for the actuator and vibration suppression loops are chosen to impart 5% damping to the structure's flexible mode in the linear region of the actuator.[8]

Case 1: $\omega_{b1} = 14.142$ rad/s $> \omega_{st}$.

For this choice of parameters, the structure's natural frequency is well below the actuator's saturation break frequency. The performance function is shown in Fig. 7. The performance function is defined on a four-dimensional domain. In Fig. 7 and in the figures that follow we have plotted this function on the subspace of initial conditions where

$$y_{st}(0) = y_{pm}(0), \text{ or, } y_r(0) = 0 \text{ and } \dot{y}_{st}(0) = \dot{y}_{pm}(0) \qquad (19)$$

This subspace serves as a basis of comparison for different actuators with widely varying parameters. Similar results are obtained for other subspaces.

Figure 7 shows that if the initial condition occurs where the performance function is zero, then the corresponding relative position response of the structure and the proof-mass, $y_r(t)$, violates the stroke limit for some value of $t > 0$. If the initial condition corresponds to a relative position response that does not violate the stroke limit for all t, then the equivalent damping is 5%.

Case 2: $\omega_{b2} = 8.165$ rad/s $= \omega_{st}$.

The performance function for this choice of parameters is similar to the performance function shown in Fig. 7 except the operating region is increased.

Case 3: $\omega_{b3} = 4.472$ rad/s $< \omega_{st}$.

In this case the saturation break frequency is well below the structure's natural frequency. Figure 8 shows the performance function for this system. Note that the equivalent damping has been reduced near the boundary of the operating region. Furthermore, the operating region is skewed near the boundary. In these regions the actuator shows pronounced nonlinear behavior due to the force saturation. This performance function is qualitatively different than the performance function in Fig. 7.

Comparison of Operating Regions

Figure 9 shows the operating region for the three cases just discussed. When the actuator's saturation break frequency is greater than the structure's natural frequency, $\omega_b > \omega_{st}$, as in case 1, the force available from the actuator is limited by the stroke length of the actuator. Here the stroke nonlinearity defines the operating region. The actuator exhibits linear behavior within the operating region because the force saturation nonlinearity is not affecting the dynamics of the actuator in the operating region. The operating region increases as the saturation break frequency increases, as shown in Fig. 9, because more of the available force is used.

When the actuator's saturation break frequency is less than the structure's natural frequency, $\omega_b < \omega_{st}$, as in case 3, the operating region takes on an irregular shape. Close to the origin the performance function matches the previous performance functions. For larger excitations, however, the force saturation nonlinearity dominates the actuator dynamics. This nonlinear response corresponds to a reduced equivalent damping at the boundaries of the operating region and the irregular shape of the operating region. In this regime limit cycles also can be observed for some sets of parameters.[3]

Table 1 Actuator and control loop parameters[a]

	ω_{bi}, rad/s	K_{va}	K_{pa}	K_{ps}	K_{vs}	md, kg-m
Case 1	14.142	0.09810	200	0	26	0.15
Case 2	8.165	0.17146	200	−70	0	0.45
Case 3	4.472	0.31305	200	0	−11.5	1.5

[a]The stroke/force saturation curve is shown in Fig. 6 for each set of parameters.

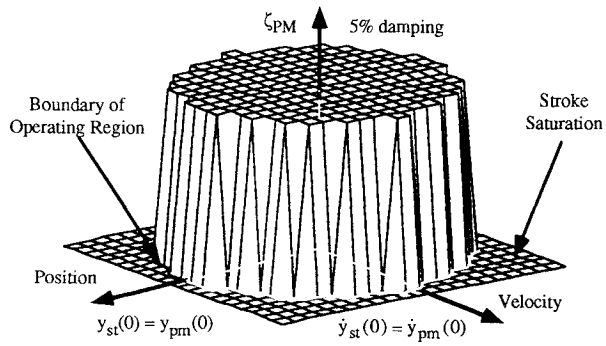

Fig. 7 Performance function for $\omega_{b1} = 14.142$ rad/s, case 1.

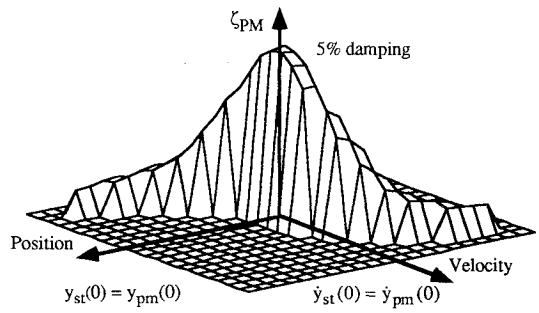

Fig. 8 Performance function for $\omega_{b3} = 4.472$ rad/s, case 3.

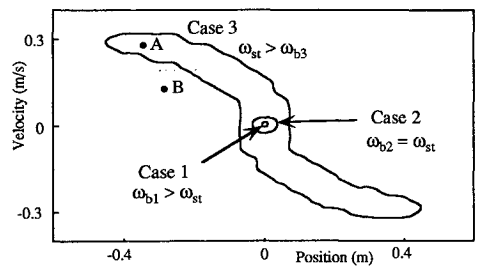

Fig. 9 Comparison of operating regions for different values of the saturation break frequency.

For concreteness, suppose that the stroke length is $d = 0.15$ m. If we choose the mass of the proof-mass to be $m = 1$ kg, then the parameters of the actuator match the parameters of case 1. If we choose the mass of the proof-mass to be 10 kg, then the parameters of the actuator match the parameters of case 3. From Fig. 9 we see that as the mass of the proof-mass increases, the operating region of the actuator increases, and the saturation break frequency decreases. When the saturation break frequency goes below the natural frequency of the structure, the operating region, while expanding, takes on an irregular shape. If a disturbance results in an initial condition into the far reaches of the operating region denoted as point A in Fig. 9, the actuator will not saturate in stroke. Such a disturbance, however, could easily result in an initial condition at point B in Fig. 9. Here the actuator will saturate in stroke. This observation suggests that, for practical purposes, the operating region for case 3 is much smaller than the computed operating region suggests. If all other parameters are held constant, increasing the mass of the proof-mass to increase the operating region leads to diminishing returns.

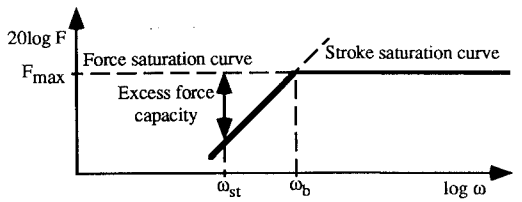

Fig. 10 Excess force capacity.

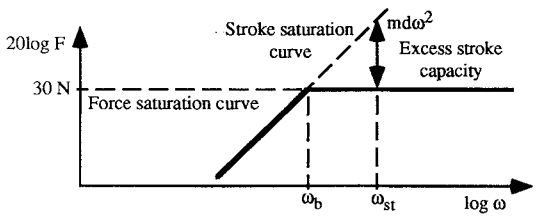

Fig. 11 Excess stroke capacity.

If the saturation break frequency is above the structure's frequency, as in case 1, the available force is underutilized as shown in Fig. 10. If the saturation break frequency is below the structure's frequency, as in case 3, the full stroke of the proof-mass is not utilized as shown in Fig. 11.

The implication of this analysis is that, for case 3, the mass of the proof-mass could be decreased without affecting the performance of the actuator. So the total mass of the actuator is reduced. Similarly, for case 1 the gain of the electromechanical subsystem of the actuator can be reduced with an attendant reduction in mass of the actuator. These observations suggest that, all other things being equal, the parameters of the proof-mass should be chosen so that the saturation break frequency is matched to the natural frequency of the structure. These results also provide guidelines for designing an actuator that is mass efficient.

These results can be used to design nonlinear control laws to prevent stroke saturation.[9–11] These results will be presented elsewhere.

Conclusions

We have examined the relationship between the parameters of a proof-massactuator and the performance of that actuator in a vibration suppression control loop for a single mode structure. The proof-mass actuator was parametrized by the mass and stroke length of the proof-mass and the maximum force available from the electromechanical subsystem. These parameters determine a stroke/force saturation curve that is characterized by the saturation break frequency. When the actuator is sized so that the saturation break frequency matches the natural frequency of the structure, the actuator is optimally utilized.

Acknowledgments

Gregory A. Zvonar was partially supported by a Fellowship from the Bradley Endowment. The authors thank E. Garcia for several useful discussions.

References

[1]Zimmerman, D. C., Horner, G. C., and Inman, D. J., "Microprocessor Controlled Force Actuator," *Journal of Guidance, Control, and Dynamics*, Vol. 11, No. 3, 1988, pp. 230–236.

[2]Hallauer, W., and Lamberson, S., "Experimental Active Vibration Damping of a Plane Truss Using Hybrid Actuation," *Proceedings of the 30th AIAA/ASME/ASCE/AHS/ASC Structures, Structural Dynamics, and Materials Conference* (Mobile, AL), AIAA, Washington, DC, 1989, pp. 80–89.

[3]Celano, T. P., "The Linear DC Motor as a Proof Mass Actuator for Vibration Suppression in Large Structures," M.S. Thesis, Bradley Dept. of Electrical Engineering, Virginia Polytechnic Inst. and State Univ., Blacksburg, VA, Sept. 1989.

[4]Ham, F., Greeley, S., and Henniges, B., "Active Vibration Suppression for the Mast Flight System," *IEEE Control Systems Magazine*, Vol. 9, 1989, pp. 85–90.

[5]Politansky, H., and Pilkey, W. D., "Suboptimal Feedback Vibration Control of a Beam with a Proof-Mass Actuator," *Journal of Guidance, Control, and Dynamics*, Vol. 12, No. 5, 1989, pp. 691–697.

[6]Sulla, J., Juang, J., and Horta, L., "Analysis and Application of a Velocity Command Motor as a Reactor Mass Actuator," *Proceedings of the AIAA Dynamics Specialist Conference* (Long Beach, CA), AIAA, Washington, DC, 1990, pp. 360–370.

[7]Haviland, J. K., Lim, T. M., Pilkey, W. D., and Politansky, H., "Control of Linear Dampers for Large Space Structures," *Journal of Guidance, Control, and Dynamics*, Vol. 13, No. 2, 1990, pp. 234–240.

[8]Lindner, D. K., Celano, T., and Ide, E., "Vibration Suppression Using a Proofmass Actuator Operating in Force/Stroke Saturation," *ASME Journal of Vibration and Acoustics*, Vol. 113, No. 4, 1991, pp. 423–433.

[9]Zvonar, G. A., Lindner, D. K., and Borojevic, D., "Nonlinear Control of a Proof-Mass Actuator to Prevent Stroke Saturation," *Proceedings of the Eighth VPI & SU Symposium on Dynamics and Control of Large Structures* (Blacksburg, VA), 1991, pp. 37–48.

[10]Zvonar, G. A., "Performance Improvement of a Proof-Mass Actuator Using Nonlinear Control," M.S. Thesis, Bradley Dept. of Electrical Engineering, Virginia Polytechnic Inst. and State Univ., Blacksburg, VA, Dec. 1991.

[11]Lindner, D. K., Zvonar, G. A., and Borojevic, D., "Limit Cycle Analysis of a Nonlinear Controller for a Proof-Mass Actuator," *Proceedings of the AIAA Dynamics Specialists Conference* (Dallas, TX), AIAA, Washington, DC, 1992, pp. 585–594.

[12]Inman, D. J., "Control/Structure Interaction: Effects of Actuator Dynamics," *Mechanics and Control of Large Structures*, edited by J. L. Junkins, Vol. 29, Progress in Astronautics and Aeronautics, AIAA, Washington, DC, 1990, pp. 507–533.